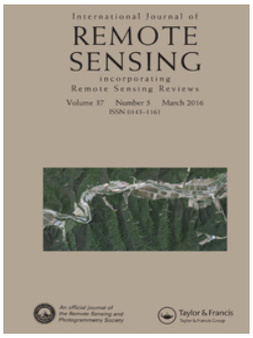

International Journal of Remote Sensing

ISSN: 0143-1161 (Print) 1366-5901 (Online) Journal homepage: http://www.tandfonline.com/loi/tres20

An efficient multi-resolution variational Retinex scheme for the radiometric correction of airborne remote sensing images

Huifang Li, Xiaojing Wang, Huanfeng Shen, Qiangqiang Yuan & Liangpei Zhang

To cite this article: Huifang Li, Xiaojing Wang, Huanfeng Shen, Qiangqiang Yuan & Liangpei Zhang (2016) An efficient multi-resolution variational Retinex scheme for the radiometric correction of airborne remote sensing images, International Journal of Remote Sensing, 37:5, 1154-1172, DOI: 10.1080/01431161.2016.1145364

To link to this article: http://dx.doi.org/10.1080/01431161.2016.1145364

Published online: 18 Feb 2016.

INTERNATIONAL JOURNAL OF REMOTE SENSING, 2016
VOL. 37, NO. 5, 1154–1172
http://dx.doi.org/10.1080/01431161.2016.1145364

Taylor & Francis
Taylor & Francis Group

An efficient multi-resolution variational Retinex scheme for the radiometric correction of airborne remote sensing images

Huifang Li[a], Xiaojing Wang[b], Huanfeng Shen[a,c], Qiangqiang Yuan[d,c] and Liangpei Zhang[e,c]

[a]School of Resource and Environmental Sciences, Wuhan University, Wuhan, PR China; [b]Baidu.com Times Technology Company, Limited, Beijing, PR China; [c]Collaborative Innovation Centre of Geospatial Technology, Wuhan, PR China; [d]School of Geodesy and Geomatics, Wuhan University, Wuhan, PR China; [e]The State Key Laboratory of Information Engineering in Surveying, Mapping and Remote Sensing, Wuhan University, Wuhan, PR China

ABSTRACT

The brightness non-uniformity caused by vignetting effects, viewing, and illumination angels in remote sensing images reduces the interpretation precision. A multi-resolution variational Retinex scheme is proposed in this paper to efficiently correct the non-uniform brightness in airborne remote sensing images. This variational Retinex model is non-linear, constrained by the grey-world assumption and the total variation regularization. A Gaussian image pyramid is used to construct the multi-resolution scheme. The multi-resolution scheme reduces the calculation burden and raises the calculation efficiency. The fast split Bregman (SB) iteration method is employed to optimize the proposed non-linear model in each level of the multi-resolution scheme. This decomposes the complicated model into several simple sub-problems and greatly improves the calculation efficiency. The multi-resolution scheme embedded with the SB iteration method was applied to both synthetic and real remote sensing images. The experimental results show that the brightness non-uniformity can be corrected, and the spectral information can be effectively restored. Moreover, the calculation efficiency is raised by about 60–110 times, compared to the traditional single-resolution solving method.

ARTICLE HISTORY
Received 21 October 2014
Accepted 16 January 2016

1. Introduction

In the acquisition process of remote sensing images, due to the sensor and environmental factors, the observed images are often degraded. Non-uniform brightness is one of the most significant degrading phenomena, which is mainly caused by the vignetting effects of lenses and some other factors, such as viewing and illumination angles (Franklin and Giles 1995; Lan et al. 2014; Li, Zhang, and Shen 2012; Shen, Peng, et al. 2015). Vignetting appears in an image as a reduction in brightness towards the image

CONTACT Huanfeng Shen shenhf@whu.edu.cn School of Resource and Environmental Sciences, Wuhan University, PR China

corners and edges (Brandtberg et al. 2003). According to Airborne Data Acquisition and Registration System 5500 data, the digital number (DN) range between the maximum near the image centre and the minimum at the image corners can vary from 15 to 45 depending on the illumination levels (Stow et al. 1996). On the other hand, the non-uniform brightness can also be caused by the viewing and illumination angles. Overall, the non-uniform brightness in a scene is recorded by DN data in aerial imagery.

The DN non-uniformity over a scene degrades the visual quality and also disturbs further applications of aerial images, such as mosaicking, feature extraction, target recognition, classification, and so on (Chen et al. 2014; Shen, Li, et al. 2015). Noted that this paper aims to correct the non-uniform brightness in a single image, though the non-uniformity also exists among different images, which is very important but using different correction schemes. It is, therefore, necessary to implement brightness correction before further application of non-uniform imagery.

Since the brightness non-uniformity is caused by multiple factors, the distribution of DN variation over the scene is anomalous. Thus, image-based correction methods are considered in this paper. Moreover, assuming only the brightness non-uniformity shall be removed without any further atmospheric correction, the methods are applied to radiance (DN) data. The non-uniformity correction is taken as a preprocessing step, aiming to normalize the distorted radiance caused by vignetting effects, viewing, and illumination angles. The correction methods mentioned in this paper can be sorted into the relative radiometric normalization, which is more suitable for qualitative analysis rather than quantitative analysis.

Several image-based methods have been introduced to correct the non-uniform brightness, including the Gaussian filter–based normalization (Elad et al. 2003; Jobson et al. 1997a, 1997b), homomorphic filtering (HF) (Nnolim and Lee 2008; Seow and Asari 2004), the perceptually inspired correction methods (Bertalmio et al. 2007; Palma-Amestoy et al. 2009), and so on. In the current methods, the non-uniformity is usually considered as additive or multiplicative noise for the signal. It varies gradually in the spatial domain, occupying the low frequency of the frequency domain. Thus, the low-pass Gaussian filter and appropriately designed homomorphic filter have both been used to estimate the global noise. However, it is hard to delineate the anomalously non-uniform brightness by the fixed filters. The perceptually inspired correction methods, which are local and image-adaptive, can optimize the results by iterations.

The perceptually inspired methods are derived from the simulation of the colour constancy of the human visual system, which refers to the colour recognition ability of human eyes under chromatic or non-uniform illumination (Jobson et al. 1997a; Ma and Osher 2010; Ng and Wang 2011; Provenzi et al. 2008). Retinex methods are a typical type of the perceptually inspired correction methods, which have been used to correct the colour distortion or brightness variation in natural images. Retinex theory supposes that the observed image is the product of the illumination component and the reflectance component (Land 1983), and the colour distortion or brightness variation is caused by the illumination component, while the information of the land surface is reflected by the reflectance component. The correction can be achieved by removing the distorted illumination component. Different models have been proposed to calculate the reflectance component directly or by estimating the optimal illumination, among which the

variational model has the advantages of integratability, extendability, and strictness (Elad et al. 2003; Kimmel et al. 2003).

The basic assumptions of Retinex theory are also adapted to optical aerial images, which usually contain more spectral bands than natural images. As the correction is carried out band by band, the band amount has no impact on the implementation. The colour of a multi-spectral data is the composition of its arbitrary three bands. The aerial data used in our experiments contain three visible bands (red, green, and blue) like natural images. Thus, colour refers to the visual effect of the images obtained in the red, green, and blue channels. We have verified the suitability of the variational correction models for remote sensing images in the previous study (Li, Zhang, and Shen 2012). The brightness variation caused by vignetting effects, lens, and illumination can be effectively corrected, and the results with uniform global brightness and enhanced local contrast can be obtained.

However, there are still two problems that need solving for the variational Retinex models. The first one is the calculation efficiency, for the costs of iterations are very high for large remote sensing images. The second one is the loss of spectral information. As the constraint for the global brightness normalization is strict, the resulting image in each band is very grey. It leads to the colour of arbitrary three band composition is not very rich. In a number of previous studies, part of the non-uniform illumination was retained in the result to keep the natural colour of the natural image (He, Sun, and Tang 2011; Kimmel et al. 2003).

Therefore, we intend to propose a simple and efficient correction method to remove the non-uniform brightness and restore the spectral information of remote sensing images. A multi-resolution variational Retinex (MVR) scheme is proposed for the non-uniformity correction, and the split Bregman (SB) iteration is introduced to improve the calculation efficiency (Goldstein and Osher 2009). A number of popular multi-resolution schemes have been proposed, including the Gaussian pyramid, the Laplacian pyramid (Burt and Adelson 1983), the wavelet pyramid (Mallat 1989), and so on. Among these multi-resolution schemes, the Gaussian pyramid is convenient and efficient, and can be used to accelerate the calculation (Kimmel et al. 2003; Ng and Wang 2011), for only a few iterations will be sufficient at the coarse layers. Thus, the Gaussian pyramid is employed in the proposed model to construct the multi-resolution correction scheme.

2. Variational Retinex model

Retinex theory supposes that a given image I is composed of the product of two different components, the reflectance component R and the illumination component L, which can be expressed as $I(x) = R(x)L(x)$, where x represents the location of a pixel. The reflectance component R describes the radiometric and spatial properties of the observing scene, which is an illumination-invariant variable. The illumination component L contributes to the global brightness variation caused by vignetting effects or other factors, which needs to be removed in the final corrected results.

To obtain the uniform image without the influence of the non-uniform illumination, we can solve the reflectance directly or by estimating the illumination first. No matter in what manner, the unknown variables are more than the functions if only $I(x) = R(x)L(x)$ is built. So, some constraints are needed to ensure the stable solutions. Moreover, to

simplify the calculation, the logarithm is usually used first to transform the multiplication to the addition, that is, $i = \ln(I)$, $r = \ln(R)$, $l = \ln(L)$, and then $i = r + l$. The spatial properties of the variables after the logarithm transformation are consistent with those before that transformation. Considering the physical properties of the reflectance and illumination components, four assumptions can be made.

(1) The illumination component is spatially smooth, as it is a global and surface-invariant variable, whose gradient can be constrained by the L2 norm (Kimmel et al. 2003), that is, $\min \sum_{\Omega} |\nabla l|^2$, where Ω refers to the image domain.
(2) The reflectance component R reflects the physical properties of the observed surface, containing edges, textures, and spatial structures, which should be reserved in the results. For the total variation (TV) has the ability to reserve details while removing noises (Rudin, Osher, and Fatemi. 1992), it is used to constrain R, that is, $\min \sum_{\Omega} |\nabla r|$.
(3) The data range of the reflectance component R is $[0, 1]$, which means that $l \geq i$ or $r \leq 0$.
(4) For visible imagery, the reflectance component R meets the Gray World (GW) rule, which assumes that the spatial average of a scene is neutral grey (Finlayson, Hordley, and Hubel 2001). Then the approximation of R to 0.5 can be used to realize the GW constraint, that is, $\sum_{\Omega} (\exp(r) - 0.5)^2$, which controls the global brightness variation of the scene.

In order to facilitate the construction of the multi-resolution scheme, the illumination is taken as an intermediate variable to solve the reflectance component in the proposed method. Details of the multi-resolution scheme are provided in the next section.

Four constraints have been constructed, among which the spatial smoothness constraint on the illumination is the strictest. This spatial property of illumination will also be utilized in the construction of the multi-resolution scheme, so we determine to estimate illumination first in our model. Based on the observation model $i = r + l$, the constraints on the reflectance can be converted to the constraints on the illumination. Thus, the second constraint can be written as $\min \sum_{\Omega} |\nabla(i - l)|$, and the fourth constraint can be written as $\sum_{\Omega} (\exp(i - l) - 0.5)^2$. Integrating the above assumptions, an energy function about the illumination can be expressed as

$$l = \arg\min_{l} F(l) = \arg\min_{l} \sum_{\Omega} (|\nabla l|^2 + \lambda_1 |\nabla(i - l)| + \lambda_2 (\exp(i - l) - 0.5)^2) \quad \text{subject to } i(x) \leq l(x), \tag{1}$$

where Ω is the support of the image, i is the observed image, l is the illumination image, x represents a pixel in the image domain, and λ_1 and λ_2 are free non-negative real parameters to control the contribution of the second and third items. It is noted that in the following equations of this paper, same symbols represent the same variables with Equation (1). The illumination l can be obtained by minimizing $F(l)$, and then the reflectance R can be obtained by the transformation $R = \exp(i - l)$.

3. Multi-resolution variational Retinex method

As mentioned before, the current variational correction methods have two shortcomings: (1) the calculation burden is high and (2) the chromatic information is lost. For the variational model, the multi-resolution scheme is an effective acceleration strategy, and the layer-by-layer calculation is also effective at preserving the chromatic information. In order to further improve the calculation efficiency, the new numeric optimization solver, the fast SB method, is used to replace the traditionalsteepest descent (SD) method. The proposed multi-resolution variational Retinex method based on split Bregman (MVRSB) aims to quickly remove the non-uniform brightness while preserving the chromatic information in the image.

3.1. *Multi-resolution scheme*

A Gaussian pyramid is used to construct the multi-resolution scheme of the variational correction model, because it is suitable to solve a variable with spatial smoothness. This is also why the correction model is a penalty function related to the illumination component.

In the Gaussian pyramid, the original image I is decomposed into a sequence of images I_k, $k \in \{0, 1, 2, 3, \ldots, N-1\}$, each of which can be regarded as an approximation of the illumination component at the corresponding scale k. The original image I is labelled as I_0. The image at scale $k+1$ is obtained by

$$I_{k+1} = g(I_k), \tag{2}$$

where $g(\cdot)$ can be expressed as

$$g(I_k(x)) = [\omega(x) * I_k(x)]_{\downarrow 2}, \tag{3}$$

$$\boldsymbol{\omega} = \begin{pmatrix} \frac{1}{16} & \frac{1}{8} & \frac{1}{16} \\ \frac{1}{8} & \frac{1}{4} & \frac{1}{8} \\ \frac{1}{16} & \frac{1}{8} & \frac{1}{16} \end{pmatrix}, \tag{4}$$

where $\boldsymbol{\omega}$ is a Gaussian kernel, $*$ represents the convolution operator, and $[\cdot]_{\downarrow 2}$ denotes the down-sampling operation by a 2:1 ratio.

In addition, another function is defined to obtain the finer-resolution image from a coarser-resolution image by

$$I_k = h(I_{k+1}), \tag{5}$$

where $h(\cdot)$ can be expressed as

$$h(I_{k+1}) = [I_{k+1}]_{\uparrow 2}, \tag{6}$$

where $[\cdot]_{\uparrow 2}$ denotes an up-sampling operation by a 1:2 ratio.

The multi-resolution brightness correction model includes three steps, as shown in Figure 1. First, the Gaussian pyramid of image i is generated. Assuming that the Gaussian pyramid of image i has N levels, each layer of the pyramid is represented as i_k, $k \in \{0, 1, 2, 3, \ldots, N-1\}$. We then start from the top layer of the pyramid i_{N-1} and obtain the coarsest illumination I_{N-1} by optimizing the penalty function. After that, the

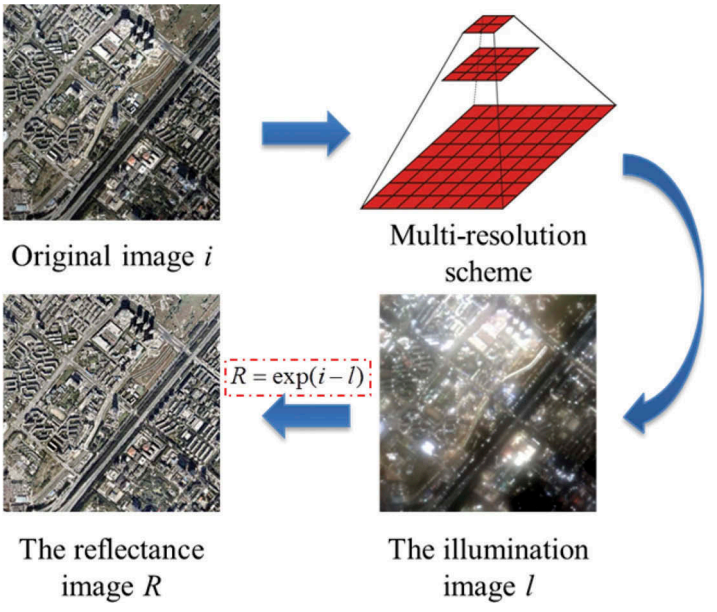

Figure 1. The overall procedure of the proposed method.

progressive circulation begins. When $N > 1$, deal I_{N-1} with the function $h(\cdot)$, and then obtain the image $I^0_{(N-2)}$, which is of the same size as i_{N-2}. The image $I^0_{(N-2)}$ is regarded as an initialization image for the next level $N-2$. At the level $N-2$, the same optimization as level $N-1$ is carried out. The above procedure is repeated until the top image i_0, to obtain the final illumination result I_0. Finally, the reflectance component R with uniform brightness can be obtained by the exponential transformation.

Summarizing the above descriptions, the procedure of the MVR model for radiometric correction is shown in Figure 1, and the details are shown in the Algorithm.

Algorithm. MVR model for radiometric correction.
Input: the observed image I.
Logarithm: $I = L \times R \xrightarrow{\ln} i = l + r$.
Gaussian pyramid generation: $i \rightarrow i_k, k \in \{0, 1, 2, 3, \ldots, N-1\}$.
Optimize from the bottom of the pyramid ($k = N-1$), as shown in the procedure in Figure 2:
if $k = N-1$,
then initialize the illumination $I^0_{N-1} = i_{N-1}$
$I_{N-1} = \arg\min_{I_{N-1}} F(I_{N-1})$.
else if $0 \le k < N-1$,
then $I^0_k = h(I_{k+1})$.
$I_k = \arg\min_{I_k} F(I_k)$.
End
Output: reflectance component in the spatial domain $R = \exp(i_0 - I_0)$.

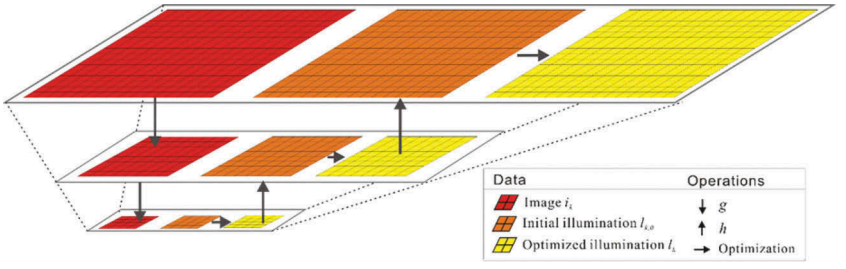

Figure 2. The multi-resolution scheme for the variational Retinex model.

Overall, the fast convergence in each layer is the key to the high efficiency of the multi-resolution scheme.

In the image pyramid, the bottom image, with the coarsest spatial resolution, contains the fewest pixels. Thus, the iterations needed for solving the coarsest illumination component are very few in the multi-resolution scheme. Moreover, since the illumination component is spatially smooth, the interpolation of the coarse illumination component can be considered as an approximation of the illumination in the finer layer. That approximation makes the iteration converge quickly in the finer layers. These are the key reasons for the high calculation efficiency of the proposed multi-resolution method. However, it should be noted that the calculation efficiency will reach a limitation with the increase of layers. First, the iterations of the optimization procedure increase when the image pyramid is high. Second, the bottom layer is too coarse to supply a good illumination initialization for next layers. Thus, more rigid iteration termination conditions have to be satisfied to get the optimal illumination component, which costs much more time.

Besides raising the calculation efficiency, the Gaussian pyramid–based multi-resolution method also performs well in colour restoration. The solution for an optimization problem is actually an approximate solution, which is related to the initialization and the numerical iteration process. The spatially smooth images are taken as the initial illumination components in the multi-resolution method, which is consistent with the physical characteristics of the illumination. Therefore, the layer-by-layer optimization results in a smoother and greyer illumination than the single-resolution optimization, and more spatial and chromatic information is preserved in the results.

3.2. *Multi-resolution variational Retinex model based on split Bregman iteration*

In order to improve the calculation efficiency further and ensure the algorithm stability, SB iteration is selected to solve the optimization problem in each layer, and is referred to as the MVRSB iteration.

In each level of the multi-resolution scheme, the minimization of $F(l)$ is a non-linear variational optimization problem, which is difficult to solve (Chen, Donoho, and Saunders 2001; Getreuer 2012; Rudin, Osher, and Fatemi. 1992). Certain iterative numerical methods can be used to obtain the approximate solution. The traditional SD method is a line search method, which is time-consuming and unstable for solving the non-linear problem. The SB iteration has been demonstrated to be an effective solver for a very

broad class of L1-regularized problems (Goldstein and Osher 2009; Yin et al. 2008). It has several advantages: (1) SB iteration converges very quickly, (2) the regularization parameter is constant, and (3) the numerical solution is stable (Cai, Osher, and Shen 2009; Goldstein and Osher 2009; Li, Zhang, and Shen 2012; Zhu and Chan 2008). The TV-regularized problem is a common example of an L1-norm problem. Therefore, the SB iteration is employed to solve the optimization problem in each layer of the multi-resolution scheme.

Due to the coupling between TV and L2 norms, solving the energy function (Equation 1) directly is hard. We wish to split the model into general problems including only L1 or L2 terms by using SB. Thus, a new variable d is introduced, $d = \nabla(i - l)$, so that we need to solve this following constrained problem:

$$\min_{l,d} \sum_{\Omega} \left(|\nabla l|^2 + \lambda_1 |d| + \lambda_2 (\exp(i - l) - 1/2)^2 \right), \text{ subject to } d = \nabla(i - l), \tag{7}$$

where i is the observed image, l is the illumination image, and d is an auxiliary variable to linearize the problem. To transform Equation (7) to an unconstrained optimization problem, the above problem can be expressed as

$$\begin{cases} (l^{j+1}, d^{j+1}) = \min\limits_{l,d} \sum\limits_{\Omega} \left(|\nabla l|^2 + \lambda_1 |d| + \lambda_2 (\exp(i - l) - 1/2)^2 + \frac{\lambda_3}{2} \left| d - \nabla(i - l) - b^j \right|^2 \right) \\ b^{j+1} = b^j + \nabla(i - l^{j+1}) - d^{j+1} \end{cases}, \tag{8}$$

where variable b is an auxiliary variable to accelerate the iteration (Goldstein and Osher 2009), j represents the iteration number, and λ_3 is a non-negative parameter to control the contribution of the last term.

Since the TV and L2 terms in the model have been split, the minimization can be performed efficiently by iteratively minimizing with respect to l and d. The two separate steps are the following:

$$\begin{cases} \text{Step 1} : l^{j+1} = \min \sum\limits_{\Omega} \left(|\nabla l|^2 + \lambda_2 (\exp(i - l^j) - 1/2)^2 + \frac{\lambda_3}{2} \left| d^j - \nabla(i - l) - b^j \right|^2 \right) \\ \text{Step 2} : d^{j+1} = \min \sum\limits_{\Omega} (\lambda_1 |d| + \frac{\lambda_3}{2} \left| d - \nabla(i - l^{j+1}) - b^j \right|^2) \end{cases}. \tag{9}$$

Thus, to solve Step 1, the fast iterative Gauss–Seidel method is used (Boyd and Vandenberghe 2004; Nocedal and Wright 2006). In Step 2, because there is no coupling between the elements of d, then the variable d can be explicitly computed by the shrinkage operator $s(\cdot)$.

$$\begin{cases} d^{j+1} = s(\nabla(i - l^{j+1}) + b^j, \lambda_1/\lambda_3) \\ s(x, \gamma) = \frac{x}{|x|} * \max(|x| - \gamma, 0) \end{cases}. \tag{10}$$

When the termination condition $\frac{\sum_{\Omega} |l^{j+1} - l^j|^2}{\sum_{\Omega} |l^j|^2} < \delta$ is met, the iteration stops, where $\sum_{\Omega} |\cdot|^2$ refers to the L2 norm of a variable, and δ is the stopping tolerance and set 10^{-3} in the experiments.

In the solving process, the original non-linear problem is split into two sub-problems, which are very easy to optimize. Both the Gauss–Seidel iteration and the shrinkage operator are very fast. Therefore, compared with the traditional gradient methods, the SB iteration is very efficient in solving the proposed variational model for radiometric correction.

4. Experiments

To verify the performance of the proposed method, experiments with both synthetic and real data were performed. The performances and running time of the multi- and single-resolution schemes were compared. Moreover, the traditional SD method and the SB iteration method were also compared. The method was developed by C++, and the trials were undertaken on a Pentium(R) Dual-Core 2 Duo desktop PC (E5200, 3.00 GHz) with 2 GB memory.

4.1. *Synthetic experiments*

A remote sensing image with uniform illumination was chosen as the original standard image for the synthetic experiments. The image contains a single band and 512 × 512 pixels, as shown in Figure 3. Two kinds of degraded images were generated: linear brightness changing along the horizontal direction, the horizon illumination, and degraded images are shown in Figures 4(*a*) and (*b*); and brightness changing along the Gaussian kernel spreading direction, as shown in Figures 5(*a*) and (*b*).

The results obtained by the existing methods, HF and Gaussian filter–based normalization, and the four methods described in this paper, single-resolution variational Retinex model based on steepest descent (SVRSD) and split Bregman (SVRSB), MVRSD, and MVRSB, are compared. The latter four methods outperform the former two methods by both subjective and objective evaluations. The peak signal-to-noise ratios (PSNRs) for the former two methods are around 21, lower than 30 obtained by the latter four

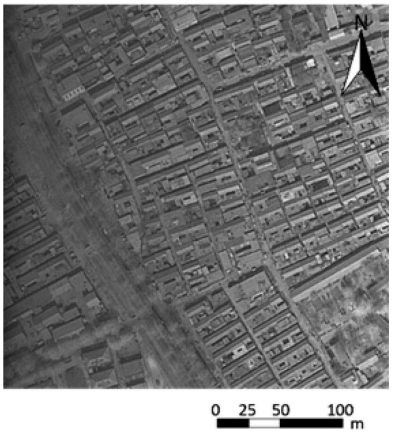

Figure 3. The original image for synthetic data.

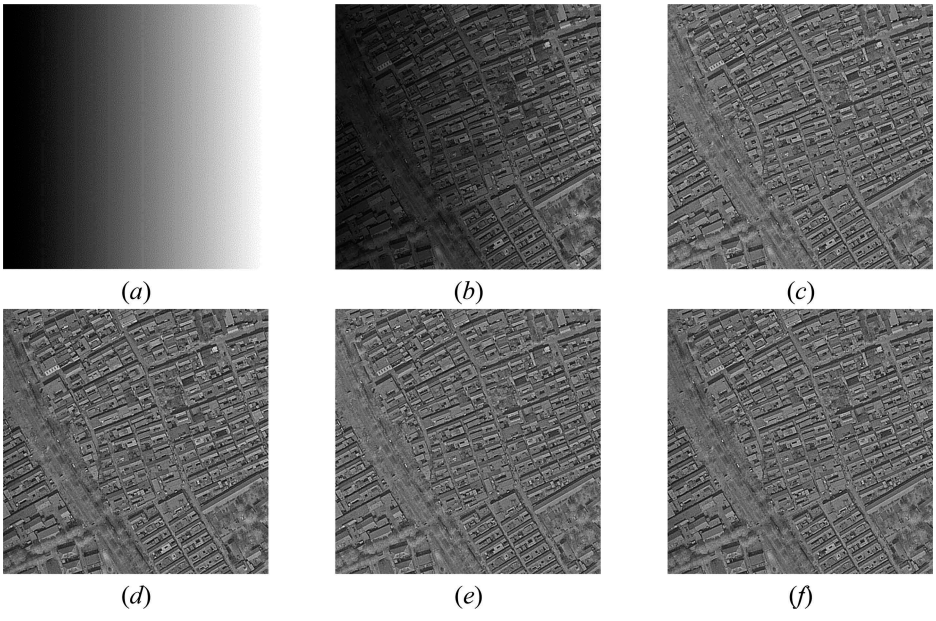

Figure 4. The horizontally degraded image and corrected results. (*a*) The horizon illumination. (*b*) The synthetic horizontally degraded image. (*c*) SVRSD. (*d*) SVRSB. (*e*) MVRSD. (*f*) MVRSB.

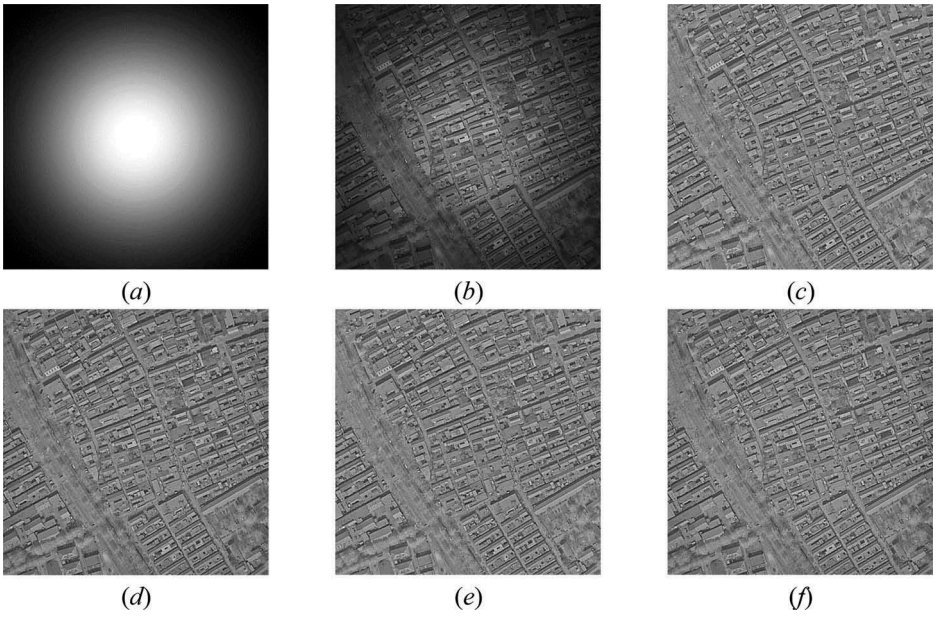

Figure 5. Gaussian degraded image and results. (*a*) Gaussian kernel spreading illumination. (*b*) Gaussian degraded image. (*c*) SVRSD. (*d*) SVRSB. (*e*) MVRSD. (*f*) MVRSB.

methods. However, the former two methods are very efficient, and the corresponding running time for the synthetic data is around 2.595 s and 2.304 s. The single-resolution method, SVRSD, is far slower than the former two. The efficiency of SVRSB and MVRSD is

Table 1. Parameters, PSNRs, and running time of the different methods for the horizontally degraded image.

	Degraded	SVRSD	SVRSB	MVRSD	MVRSB
λ_1	–	0.001	0.001	0.001	0.007
λ_2	–	0.04	0.05	0.08	0.09
λ_3	–	–	0.01	–	0.01
Δt	–	0.075	–	0.075	–
PSNR	13.72	29.17	29.15	30.63	30.00
RMSE	52.55	8.87	8.89	7.50	8.06
SSIM	0.782	0.992	0.991	0.996	0.992
DGA	23.83	2.04	1.99	3.84	3.24
Time (s)	–	250.28	33.11	16.45	3.27

– Means that the current cell value does not exist.

raised by the numerical optimization and the multi-resolution strategy, respectively. The running time of MVRSB is close to the former two, and meanwhile MVRSB yields results with higher PSNRs. The running time for the latter four methods is listed in Table 1.

Corrected images are presented and compared in Figures 4 and 5, and the parameter settings for each result are listed in Table 1. The parameters were determined based on the multiple tests on the synthetic data. One parameter varied when the others kept constant, and it was set when the highest PSNR was obtained.

By visual evaluation, it can be seen from Figure 4 that the non-uniform brightness caused by the linear illumination has been corrected in the results. Considering the efficiency of the different methods, the running time of the single- and multi-resolution methods is listed and analysed (see Table 1). To be fair, the running time was the average over 10 runs and were recorded when the same or approximate PSNRs (near 30) were obtained by the four methods. It can be seen that the running time of SVRSB is almost one-seventh that of SVRSD, the running time of MVRSD is nearly one-fifteenth that of SVRSD, and the running time of MVRSB is one-eightieth that of SVRSD. This indicates that both multi-resolution scheme and SB iteration can greatly improve the calculation efficiency of the proposed model, and the combination of these two measures is an efficient way to speed up the correction process. The Gaussian degraded image, shown in Figure 5(*b*), has brighter centre than the surroundings. The corrected results of the Gaussian degraded image are shown in Figures 5(*c*)–(*f*). It is very clear that the non-uniform brightness in the four results is effective. Table 2 shows the parameters, the PSNRs, and the running time. It can be seen that when the PSNRs of the four results are near 29, the running time of MVRSD and SVRSB is much less than that of SVRSD.

Table 2. The parameter settings, PSNRs, and running time for the Gaussian degraded synthetic data.

	Degraded	SVRSD	SVRSB	MVRSD	MVRSB
λ_1	–	0.001	0.001	0.001	0.05
λ_2	–	0.04	0.05	0.12	0.09
λ_3	–	–	0.01	–	0.01
Δt	–	0.075	–	0.075	–
PSNR	12.47	29.19	29.17	29.14	29.10
RMSE	60.71	8.85	8.88	8.90	8.94
SSIM	0.717	0.992	0.991	0.993	0.991
DGA	16.10	2.10	2.04	3.57	4.04
Time (s)	–	240.58	33.80	18.22	3.90

– Means that the current cell value does not exist.

Moreover, it is also very clear that the running time of the MVRSB method is much less than those of the other three methods, and is almost one-sixtieth that of SVRSD. Additionally, other three quantitative assessment indexes are also used to evaluate the correction results, including root mean square error (RMSE), structural similarity (SSIM), and distortion of gain adjustment (DGA), as listed in Tables 1 and 2 (Pal and Porwal 2015; Wang et al. 2004). The results suggest that these four Retinex-based methods are effective on the brightness correction, and the correction results are similar when the running time is recorded and compared.

Through the synthetic experiments and quantitative assessments, it can be seen that the proposed variational model is effective in correcting different types of non-uniform brightness. The integration of the multi-resolution scheme and the SB iteration is very efficient for obtaining the optimal uniform results. It advocates the usage of the proposed method for the large-scale remote sensing data. However, the distribution of the brightness may not follow any particular kind of formula in the real scenes. Thus, more experiments on aerial data are carried out to test the proposed method.

4.2. *Aerial data*

Three aerial images with non-uniform brightness were employed. Figure 6(*a*) shows the first real remote sensing image, with 600×400 pixels and three visible bands (red, green, and blue), clipped from a large scene. It can be seen that the brightness in the top left part is darker than that in the bottom right part, which can be mainly attributed to the vignetting effects. The corrected results are shown in Figures 6(*b*)-(*e*), (*f*) is the illumination calculated by MVRSB, and the parameter settings for the different results are listed in Table 3. Note that the layer numbers for the multi-resolution methods are all 4 and the determination of the layer number will be explored in Section 4.3.

By visual evaluation, the brightness non-uniformity between the top left part and the bottom right part has been removed in all four results. Moreover, it is clear that the colours (combination of images from red, green, and blue channels) of the four results are different. More chromatic information is preserved in the results from multi-resolution methods, as shown in Figures 6(*d*) and (e), which are more visually natural than Figures 6(*b*) and (*c*). For example, the vegetation (which is an important factor affecting human visual feeling) in the multi-resolution results is much greener than that in the single-resolution results. With regard to the calculation efficiency aspect, much time can be saved by the multi-resolution scheme and the SB iteration, as listed in Table 3. The running time of MVRSB is about one-seventieth that of SVRSD. The above results suggest that MVRSB is an effective and efficient brightness correction method, with good colour preservation at the same time. In order to further verify the effect of the proposed correction method, experiments on another two aerial images are carried out. The second image contains 1000×1000 pixels and three bands, shown in Figure 7(*a*), and the third image contains 950×600 pixels and three bands, shown in Figure 8(*a*). Through the experimental testing, the parameter setting of the proposed method was found to be robust with regard to the aerial data covering urban areas. Therefore, the parameter settings for these two images were kept the same as with the first image.

The results for the second and the third aerial images are shown in Figures 7(*b*)-(*f*) and 8 (*b*)-(*f*), and the running time is listed in Table 4. By visual assessment, the same conclusion can be reached as for the first image, that the multi-resolution methods yield better results,

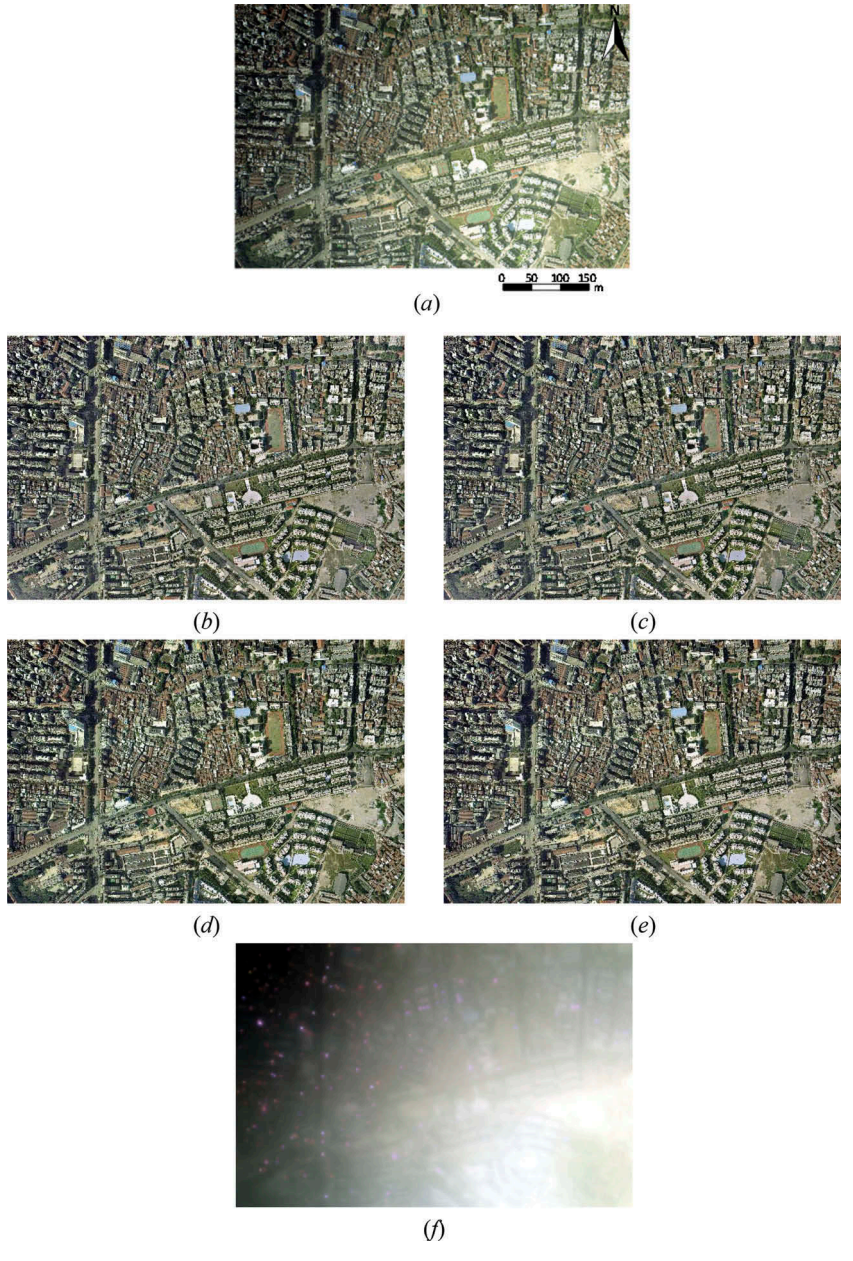

Figure 6. The first aerial image and the results. (*a*) The first aerial image. (*b*) SVRSD. (*c*) SVRSB. (*d*) MVRSD. (*e*) MVRSB. (*f*) The illumination component calculated by MVRSB.

Table 3. Parameters and running time of the different solutions for the first aerial image.

	SVRSD	SVRSB	MVRSD	MVRSB
λ_1	0.001	0.001	0.001	0.001
λ_2	0.01	0.01	0.01	0.01
λ_3	–	0.01	–	0.01
Δt	0.075	–	0.05	–
Time (s)	574.94	89.81	40.31	5.01

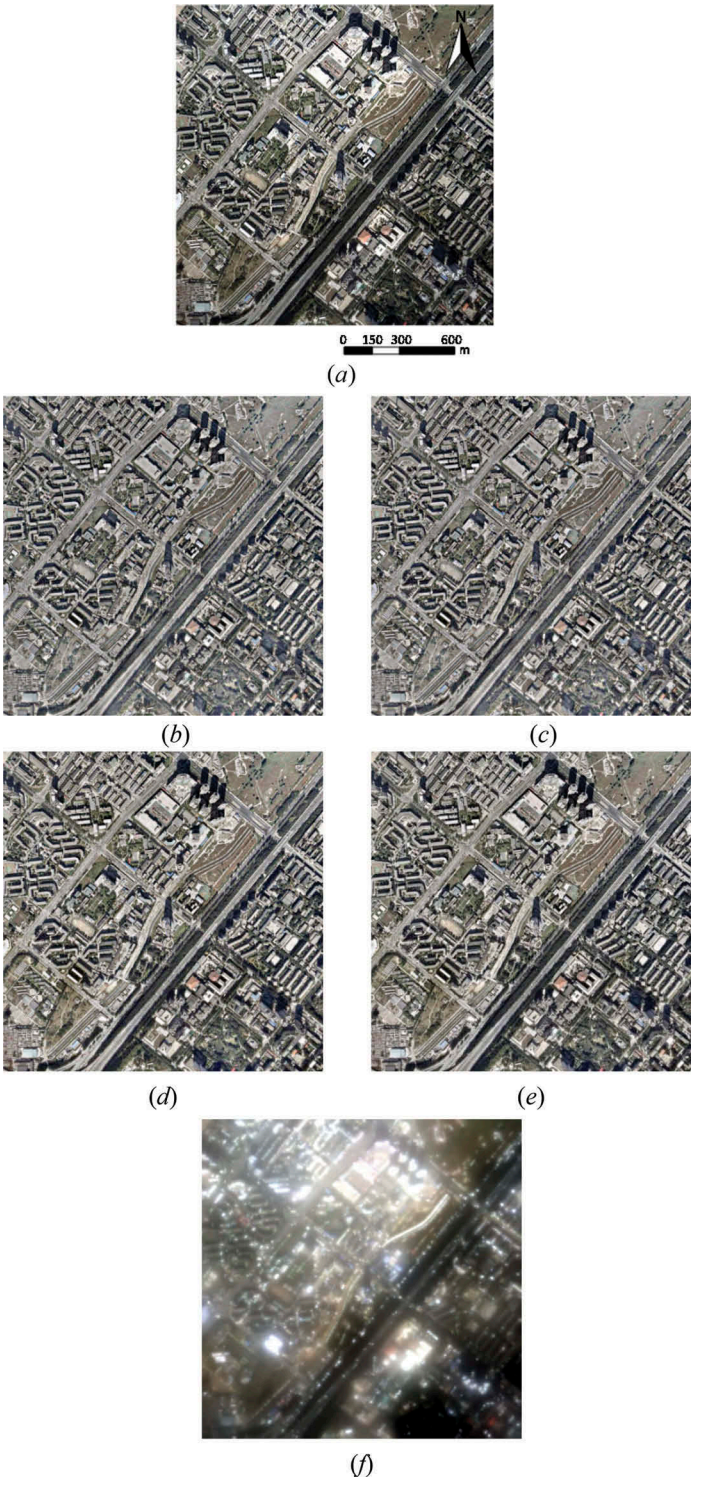

Figure 7. The second aerial image and the results. (*a*) The second aerial image. (*b*) SVRSD. (*c*) SVRSB. (*d*) MVRSD. (*e*) MVRSB. (*f*) The illumination component calculated by MVRSB.

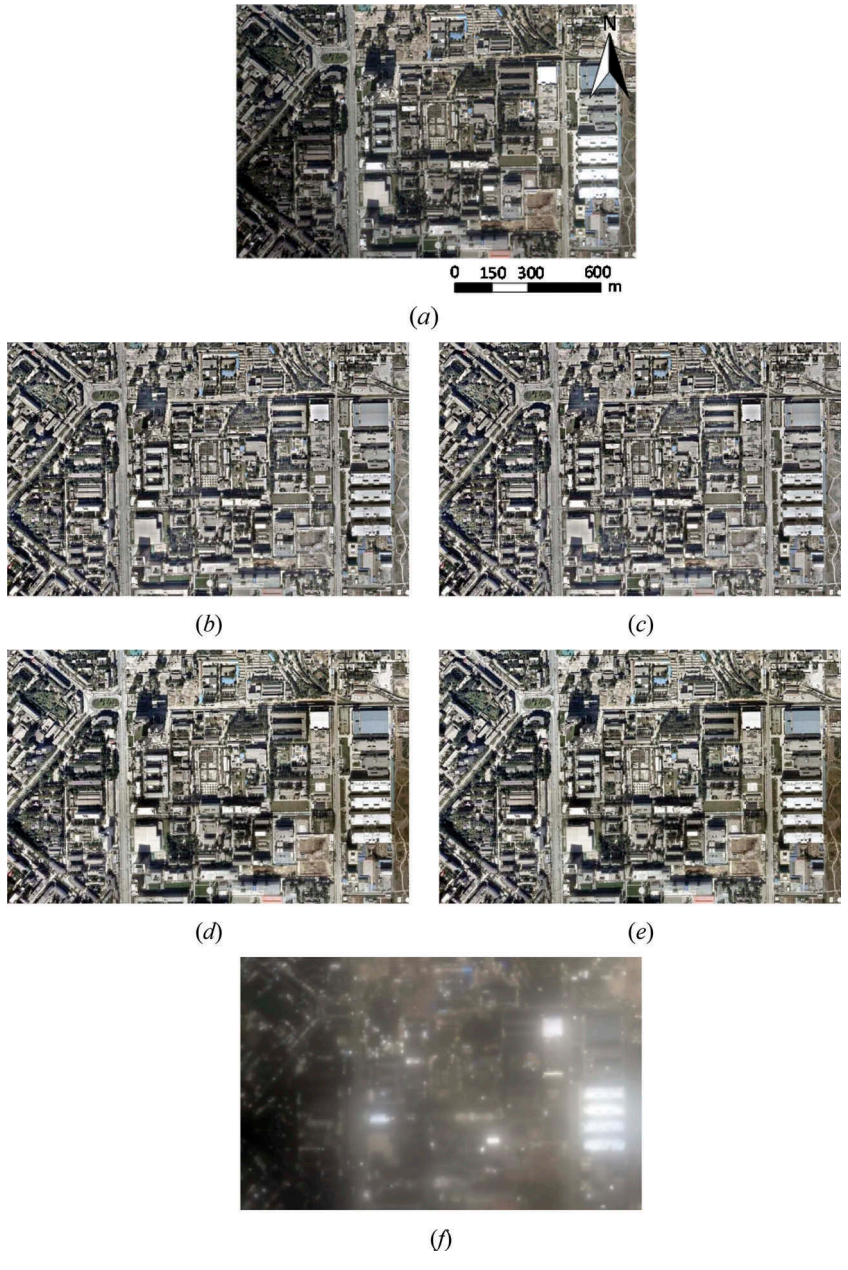

Figure 8. The third aerial image and the results. (*a*) The third aerial image. (*b*) SVRSD. (*c*) SVRSB. (*d*) MVRSD. (*e*) MVRSB. (*f*) The illumination component calculated by MVRSB.

Table 4. The running time of the second and third aerial images.

Time (s)	SVRSD	SVRSB	MVRSD	MVRSB
Data set II	3075.33	417.86	377.92	46.61
Data set III	1649.59	216.95	145.86	19.73

Table 5. The running time for different layer numbers with the three aerial images.

Layer number	2	3	4	5	6	7	8	9	10
Data set I	15.63	6.90	**5.06**	49.18	161.97	170.81	183.28	189.46	203.74
Data set II	80.48	53.81	**46.12**	55.07	70.03	91.55	127.60	195.96	266.20
Data set III	43.69	22.91	**20.43**	21.46	23.15	25.02	38.02	122.23	146.37

The least running time is in bold.

with uniform brightness and more adequate chromatic information, than the single-resolution methods. Table 4 shows the running time of the two experiments on these two aerial data. Compared with the traditional single-resolution SVRSD, MVRSB saves 80% more time.

Integrating the experiments on both synthetic and real aerial data, it can be concluded that the multi-resolution method is efficient for not only raising the calculation efficiency, but also improving the colour preservation.

4.3. *Layer number determination*

How many layers is the best is a problem for the multi-resolution-based methods. In order to explore the influence of the layer number in the multi-resolution scheme, a series of experiments on the three aerial data with different layer numbers was carried out. The corresponding running time for the MVRSB method using different numbers of layers is listed in Table 5.

Here, we take the second aerial image and MVRSB method as an example to analyse the influence of the layer number. The layer number was changed from 1 to 10, in which 1 is the single-resolution result, as shown in Figure 7(*c*), and the results of 2–10 layers are shown in Figure 9. The brightness variation has been corrected in all the different results. However, it can be observed that the colour becomes more and more natural as the layer number increases from 1 to 4. This can be attributed to the ability of the multi-resolution method to produce smoother and greyer illumination components. When the layer number is greater than 4, the visual effect of the results is constant. However, with the increase of the layer number, the size of the bottom layer becomes very small. The more rigid iteration termination conditions have to be satisfied to get the optimal illumination component, which means that much more time is needed (as listed in Table 5). The running time is the shortest when the layer number equals 4 for all the three images used in our experiments. Thus, integrating the visual effects and running time, 4 is taken as the best layer number for our method.

5. Conclusions

The proposed MVR method is effective and efficient for correcting the non-uniform brightness in remote sensing images. It has been validated that the multi-resolution scheme is not only an acceleration strategy, but also an effective colour preservation measure, by experimenting on both synthetic and aerial data. The SB iteration is appropriate for optimizing the sub-problems in each layer. The integration of the multi-resolution scheme and the SB iteration yields satisfactory uniform results by costing less time than other methods. Moreover, the best layer number has also been discussed and demonstrated to be stable for different images. Based on the running time, the proposed MVRSB method can save 80% more time than the traditional SVRSD method. Thus, the method should also be possible to process larger data, which will be explored in our future study.

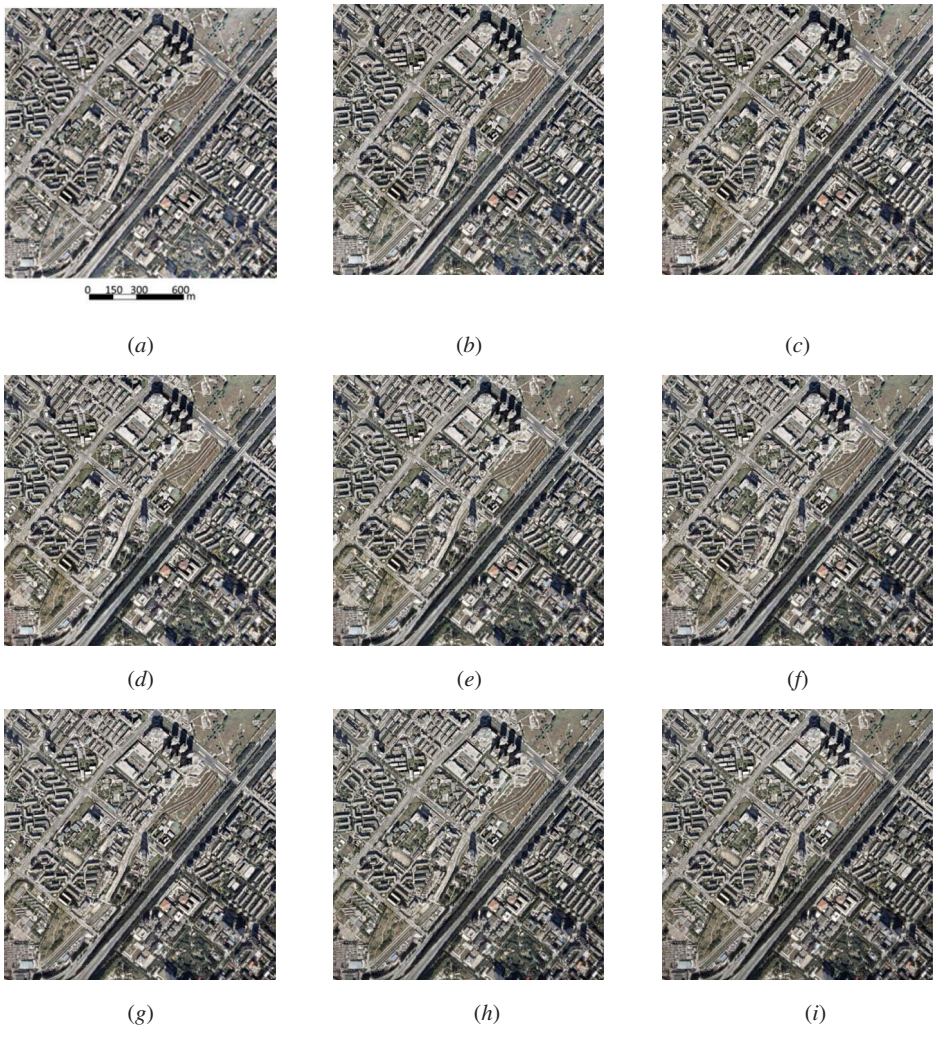

Figure 9. Results of different layer numbers for the second aerial image. Results (*a*)–(*i*), respectively, correspond to layer numbers of 2–10.

Disclosure statement

No potential conflict of interest was reported by the authors.

Funding

This research was supported by the National Natural Science Foundation of China [41422108]; the National Natural Science Foundation of China [41401396]; the Wuhan Science and Technology Program [2013072304010825]; the Natural Science Foundation of Hubei Province, China [2014CFB702]; the Fundamental Research Funds for the Central Universities [2042014kf0045].

References

Bertalmio, M., V. Caselles, E. Provenzi, and A. Rizzi. 2007. "Perceptual Color Correction Through Variational Techniques." *IEEE Transactions on Image Processing* 16 (4): 1058–1072. doi:10.1109/TIP.2007.891777.

Boyd, S., and L. Vandenberghe. 2004. *Convex Optimization*. Cambridge: Cambridge University Press.

Brandtberg, T., J. B. McGraw, T. A. Warner, and R. E. Landenberger. 2003. "Image Restoration Based on Multiscale Relationships of Image Structures." *IEEE Transactions on Geoscience and Remote Sensing* 41 (1): 102–110. doi:10.1109/TGRS.2002.808059.

Burt, P. J., and E. H. Adelson. 1983. "The Laplacian Pyramid as a Compact Image Code." *IEEE Transactions on Communications* 31 (4): 532–540. doi:10.1109/TCOM.1983.1095851.

Cai, J.-F., S. Osher, and Z. Shen. 2009. "Split Bregman Methods and Frame Based Image Restoration." *Multiscale Modeling & Simulation* 8 (2): 337–369. doi:10.1137/090753504.

Chen, C., Z. Chen, M. Li, Y. Liu, L. Cheng, and Y. Ren. 2014. "Parallel Relative Radiometric Normalisation for Remote Sensing Image Mosaics." *Computers & Geosciences* 73 (12): 28–36. doi:10.1016/j.cageo.2014.08.007.

Chen, S. S., D. L. Donoho, and M. A. Saunders. 2001. "Atomic Decomposition by Basis Pursuit." *SIAM Review* 43 (1): 129–159. doi:10.1137/S003614450037906X.

Elad, M., R. Kimmel, D. Shaked, and R. Keshet. 2003. "Reduced Complexity Retinex Algorithm via the Variational Approach." *Journal of Visual Communication and Image Representation* 14 (4): 369–388. doi:10.1016/S1047-3203(03)00045-2.

Finlayson, G. D., S. D. Hordley, and P. M. Hubel. 2001. "Color by Correlation: A Simple, Unifying Framework for Color Constancy." *IEEE Transactions on Pattern Analysis and Machine Intelligence* 23 (11): 1209–1221. doi:10.1109/34.969113.

Franklin, S. E., and P. T. Giles. 1995. "Radiometric Processing of Aerial and Satellite Remote-Sensing Imagery." *Computers & Geosciences* 21 (3): 413–423. doi:10.1016/0098-3004(94)00085-9.

Getreuer, P. 2012. "Rudin-Osher-Fatemi Total Variation Denoising Using Split Bregman." *Image Processing On Line* 2 (5): 74–95. doi:10.5201/ipol.

Goldstein, T., and S. Osher. 2009. "The Split Bregman Method for L1-Regularized Problems." *SIAM Journal on Imaging Sciences* 2 (2): 323–343. doi:10.1137/080725891.

He, K., J. Sun, and X. Tang. 2011. "Single Image Haze Removal Using Dark Channel Prior." *IEEE Transactions on Pattern Analysis and Machine Intelligence* 33 (12): 2341–2353. doi:10.1109/TPAMI.2010.168.

Jobson, D. J., Z.-U. Rahman, and G. A. Woodell. 1997a. "A Multiscale Retinex for Bridging the Gap between Color Images and the Human Observation of Scenes." *IEEE Transactions on Image Processing* 6 (7): 965–976. doi:10.1109/83.597272.

Jobson, D. J., Z.-U. Rahman, and G. A. Woodell. 1997b. "Properties and Performance of a Center/Surround Retinex." *IEEE Transactions on Image Processing* 6 (3): 451–462.

Kimmel, R., M. Elad, D. Shaked, R. Keshet, and I. Sobel. 2003. "A Variational Framework for Retinex." *International Journal of Computer Vision* 52 (1): 7–23. doi:10.1023/A:1022314423998.

Lan, X., H. Shen, L. Zhang, and Q. Yuan. 2014. "A Spatially Adaptive Retinex Variational Model for the Uneven Intensity Correction of Remote Sensing Images." *Signal Processing* 101 (8): 19–34. doi:10.1016/j.sigpro.2014.01.017.

Land, E. H. 1983. "Recent Advances in Retinex Theory and Some Implications for Cortical Computations: Color Vision and the Natural Image." *Proceedings of the National Academy of Sciences of the United States of America* 80 (16): 5163–5169. doi:10.1073/pnas.80.16.5163.

Li, H., L. Zhang, and H. Shen. 2012. "A Perceptually Inspired Variational Method for the Uneven Intensity Correction of Remote Sensing Images." *IEEE Transactions on Geoscience and Remote Sensing* 50 (8): 3053–3065. doi:10.1109/TGRS.2011.2178075.

Ma, W., and S. Osher, 2010. *A TV Bregman Iterative Model of Retinex Theory*. UCLA CAM Report, 1–13. Los Angeles, CA: Department of Mathematics, UCLA.

Mallat, S. G. 1989. "A Theory for Multiresolution Signal Decomposition: The Wavelet Representation." *IEEE Transactions on Pattern Analysis and Machine Intelligence* 11 (7): 674–693. doi:10.1109/34.192463.

Ng, M. K., and W. Wang. 2011. "A Total Variation Model for Retinex." *SIAM Journal on Imaging Sciences* 4 (1): 345–365. doi:10.1137/100806588.

Nnolim, U., and P. Lee. 2008. "Homomorphic Filtering of Colour Images Using a Spatial Filter Kernel in the HSI Colour Space." In *Victoria, Columbia, Canada, Instrumentation and Measurement Technology Conference Proceedings*, 1738–1743. Piscataway Township, NJ: IEEE.

Nocedal, J., and S. J. Wright. 2006. *Numeric Optimization*, 245–269. New York: Springer.

Pal, M. K., and A. Porwal. 2015. "A Local Brightness Normalization (LBN) Algorithm for Destriping Hyperion Images." *International Journal of Remote Sensing* 36 (10): 2674–2696. doi:10.1080/01431161.2015.1043761.

Palma-Amestoy, R., E. Provenzi, M. Bertalmio, and V. Caselles. 2009. "A Perceptually Inspired Variational Framework for Color Enhancement." *IEEE Transactions on Pattern Analysis and Machine Intelligence* 31 (3): 458–474. doi:10.1109/TPAMI.2008.86.

Provenzi, E., C. Gatta, M. Fierro, and A. Rizzi. 2008. "A Spatially Variant White-Patch and Gray-World Method for Color Image Enhancement Driven by Local Contrast." *IEEE Transactions on Pattern Analysis and Machine Intelligence* 30 (10): 1757–1770. doi:10.1109/TPAMI.2007.70827.

Rudin, L. I., S. Osher, and E. Fatemi. 1992. "Nonlinear Total Variation Based Noise Removal Algorithms." *Physica D: Nonlinear Phenomena* 60 (1–4): 259–268. doi:10.1016/0167-2789(92)90242-F.

Seow, M., and V. K. Asari. 2004. "Homomorphic Processing System and Ratio Rule for Color Image Enhancement." In *Budapest, International Joint Conference on Neural Networks*, 2507–2511. Piscataway Township, NJ: IEEE.

Shen, H., X. Li, Q. Cheng, C. Zeng, G. Yang, H. Li, and L. Zhang. 2015. "Missing Information Reconstruction of Remote Sensing Data: A Technical Review." *IEEE Geoscience and Remote Sensing Magazine* 3 (3): 61–85. doi:10.1109/MGRS.2015.2441912.

Shen, H., L. Peng, L. Yue, Q. Yuan, and L. Zhang. 2015. "Adaptive Norm Selection for Regularized Image Restoration and Super-Resolution." *IEEE Transactions on Cybernetics*. doi:10.1109/TCYB.2015.2446755.

Stow, D., A. Hope, A. T. Nguyen, S. Phinn, and C. A. Benkelman. 1996. "Monitoring Detailed Land Surface Changes Using an Airborne Multispectral Digital Camera System." *IEEE Transactions on Geoscience and Remote Sensing* 34 (5): 1191–1203. doi:10.1109/36.536536.

Wang, Z., A. C. Bovik, H. R. Sheikh, and E. P. Simoncelli. 2004. "Image Quality Assessment: From Error Visibility to Structural Similarity." *IEEE Transactions on Image Processing* 13 (4): 600–612. doi:10.1109/TIP.2003.819861.

Yin, W., S. Osher, D. Goldfarb, and J. Darbon. 2008. "Bregman Iterative Algorithms for L_1-Minimization with Applications to Compressed Sensing." *SIAM Journal on Imaging Sciences* 1 (1): 143–168. doi:10.1137/070703983.

Zhu, M., and T. Chan, 2008. *An Efficient Primal-Dual Hybrid Gradient Algorithm for Total Variation Image Restoration*. UCLA CAM Report, 8–34. Los Angeles, CA: Department of Mathematics, UCLA.